physica **pss** status solidi a
www.pss-a.com

applications and materials science

Photoluminescence associated with {113} defects in oxygen-implanted silicon

N. A. Sobolev[*,1], **A. E. Kalyadin**[1], **E. I. Shek**[1], **K. F. Shtel'makh**[1,2], **V. I. Vdovin**[3], **A. K. Gutakovskii**[3,4], and **L. I. Fedina**[3,4]

[1] Ioffe Institute, Polytekhnicheskaya 26, 194021 St. Petersburg, Russia
[2] Peter the Great Saint-Petersburg Polytechnic University, Polytekhnicheskaya 29, 195251 St. Petersburg, Russia
[3] Rzhanov Institute of Semiconductor Physics, pr. Lavrentieva 13, 630090 Novosibirsk, Russia
[4] Novosibirsk State University, Pirogova St. 2, 630090 Novosibirsk, Russia

[*] Corresponding author: e-mail nick@sobolev.ioffe.rssi.ru, Phone: +7 812 297 3885, Fax: +7 812 297 1017

The dependences of photoluminescence (PL) and the structure of {113} defects induced in n-Cz-Si (100) wafers by implantation of 350 keV O^+ ions at a dose of 3.7×10^{14} cm^{-2} on the annealing time at 700 °C for 0.5–2.0 h in a chlorine-containing atmosphere have been studied in detail. Extended defects were examined by high-resolution transmission electron microscopy (HRTEM) on cross-sectional samples. HRTEM evidences that {113} defects dominate in all the samples under study. A shift of the PL band from 920 to 903 meV ("903" line, R-line, or 1370 nm line) was observed with increasing annealing time, which suggests a strong change of the {113} defect structure. According to the Geometrical Phase Method used for the measurements of lattice deformations around the {113} defects observed by HRTEM, this change is related to a transformation of a vacancy-type {113} defect to an interstitial one. The effect of the measurement temperature on the main parameters of R-line has been studied, too. A sample annealed for 1 h has some characteristic features of the temperature dependence of the PL intensity: it increases with activation energy of 19.1 meV at low temperatures and decreases with deactivation energies of 32.2 and 175.5 meV at higher temperatures. With the increasing temperature, the luminescence peak shifts by the same energy as the forbidden gap width, while the FWHM of the line grows linearly.

© 2017 WILEY-VCH Verlag GmbH & Co. KGaA, Weinheim

1 Introduction The optical properties of {113} defects in silicon have been of interest due to their potential applicability in fabrication of Si-based light-emitting diodes [1]. The well-known technological rod-like {113} defects produced by heat treatment of Cz-Si and by electron or ion irradiation have been studied for more than three decades [2–6]. These defects were especially well understood in the ultra-shallow p–n junctions because they can be related to the enhanced transient diffusion of boron in Si [7, 8]. It was reported that, in Cz-Si annealed at 650 °C for a long time, R (903 meV, 1370 nm) photoluminescence (PL) line can be attributed to the presence of {113} defects [4, 5]. This conclusion was based on the correlation between the intensity of R line and the concentration of etch pits at various annealing durations. Later, the relationship between the formation of {113} defects and the R line was confirmed for self-ion implanted Cz-Si subjected to a relatively short annealing at higher temperatures [9, 10]. In particular, two broad bands are observed at 938 and 891 meV, irrespective of the fluence and type of ions after the 600 °C annealing [11, 12]. The annealing above 600 °C gives rise to a sharp R line attributed to {113} defects [9–13]. A correlation between the appearance of R line and the size and concentration of {113} defects was also observed in Ref. [13]. In addition, the formation and evolution of the {113} defects depended on the time of annealing at 700 °C, but no simple correlation was found between the density and size of these defects and the intensity of R line [13]. It was concluded that, while the presence of {113} defects is essential for R luminescence line to be observed, both very small {113} defects at short (10–20 min) annealing durations and fully developed {113} defects at long annealing times do not contribute to this luminescence. It was assumed that the local (strained) environment around defects, doping level, and impurities in the silicon substrate may all affect the intensity of the R line.

Phys. Status Solidi A 214, No. 7 (2017)

(2 of 8) 1700317

It is important to note that the PL associated with {113} defects induced by ion implantation is usually considered in terms of the interstitial concept (+1 model), which is based on the excess of self-interstitials that emerge during annealing in dopant-implanted silicon [8, 14]. It is believed that these self-interstitials are clustered in {113} habit planes similarly to those in electron-irradiated silicon, as found by S. Takeda for {113} defects induced at a temperature of 450 °C in a high-voltage electron microscope [3]. However, comparison of HRTEM images of {113} defects, observed in different studies upon electron irradiation and ion implantation [3, 6, 9, 10, 13, 14], shows that the implantation-related defects cannot be interpreted unambiguously as the {113} defects of the interstitial type. Moreover, *in situ* HRTEM irradiation experiments (JEOL-4000EX operated at 400 keV) at room temperature demonstrate a strong {113} defect structure variability between vacancy − amorphous − interstitial types depending on a local concentration of point defects (intensity of electron irradiation, foil thickness, etc.) [6]. This suggests that an aggregation of intrinsic point defects (vacancies and self-interstitials) on {113} planes can be observed in ion-implanted Si, too. More extended discussion on the universality of the {113} habit plane for aggregation of vacancies and self-interstitials, irrespective of the method of their generation in Si can be found in Ref. [15].

In the last year, we have observed the appearance of R luminescence line in Cz-Si upon oxygen ion implantation and subsequent annealing [16]. However, we did not study defect structure in the samples. In the present study, we examine the transformation of R line and lattice deformations (strains) introduced by {113} defects in oxygen-implanted silicon in relation to the heat treatment duration. We also report results concerning the effect of a measurement temperature on the main parameters of R line.

2 Experimental As initial samples served p^+-n structures on an n-Cz-Si(100) substrate with resistivity of $4.5\,\Omega$ cm. The p^+-n junction was formed by diffusion of boron atoms from the gas phase. The surface concentration of boron and the depth of the p^+-n junction were $\sim 10^{20}\,cm^{-3}$ and ~ 50 nm, respectively. The implantation of 350 keV O^+ ions at a non-amorphizing dose of $3.7 \times 10^{14}\,cm^{-2}$ was carried out on the side of the p^+-n junction at room temperature at an angle of $7°$ in order to avoid the channeling effect. The projected range of the O^+ ions was calculated with the SRIM program [17] to be 790 nm. Thus, the main part of the oxygen ions was implanted to a larger depth, compared with the p^+-n junction. Isothermal annealing were performed at 700 °C for 0.5, 1, 1.5, and 2 h in an oxygen flow saturated with carbon tetrachloride vapor at a concentration of 1 mol.% (chlorine-containing atmosphere). The annealings led to a transformation of structural defects and formation of luminescence centers. The PL was excited by a solid-state laser at a wavelength of 532 nm (beam diameter ~ 2 mm, intensity 2–60 mW) and recorded with an MDR-23 automated

spectrometer and an InGaAs photodetector at wavelengths in the range from 1000 to 1650 nm at temperatures of 4.2–140 K. The resolution of the setup for PL measurements was 5 nm. A sample was placed in an UTREKS cryostat, which made it possible to maintain the temperature at within ± 0.2 K. The parameters of R luminescence line (intensity, peak position of a line, and full width at half maximum, FWHM) were determined by fitting a luminescence line with a Gaussian curve. The investigations of the {113} defect structure in (110) cross-sectional specimens were carried out by the means of the JEOL-4000EX transmission electron microscope (point to point resolution limit − 0.17 nm, spherical aberration coefficient $Cs = 1$ mm) operated at 400 kV and the Titan 80–300 one operated at 300 kV for both STEM and HREM ($Cs = 10\,\mu m$) modes. We used STEM mode (point-to-point resolution limit − 0.14 nm) to detect the distribution of {113} defects in cross-sections of implanted layers. The geometrical phase method (GPA) for the first time proposed in Ref. [18] and generalized later in Ref. [19] was applied to analyze lattice deformations around {113} defects observed by HRTEM mode at various annealing stages. HRTEM images have been obtained under optimal conditions (Scherzer defocus (−45) nm at 400 keV for JEOL-4000EX (Fig. 3, column "c") and $Cs = 10\,\mu m$, defocus (−160) Å at 300 keV for the Titan 80–300).

3 Results and discussion The PL spectra at 78 K of the samples implanted with oxygen ions and then annealed at a temperature of 700 °C in a chlorine-containing atmosphere for 0.5–2 h are shown in Fig. 1. Two broad lines peaked at ~ 919 and ~ 785 meV dominate in the luminescence spectra after the annealing for 0.5 h. The lines belong to defects formed predominantly from silicon self-interstitials at the initial annealing stage of the irradiated samples [20].

With the increasing annealing time, the spectra start to be dominated by a narrow line at ~ 903 meV (R line), which is associated with {113} defects [4, 5, 9–13, 16]. In samples annealed for 1–2 h, the energy position of the line remains practically constant. The maximum intensity of the line is observed in the sample annealed for 1 h. An increase in the annealing time is followed by a decrease in the line intensity and by the appearance of a higher energy shoulder. This additional peak is redshifted. The peak was previously observed in silicon-ion-implanted samples at high implantation doses [9]. Low-intensity near-band-edge (intrinsic) luminescence lines were observed in the PL spectra of all the oxygen-ion-implanted and annealed samples (not shown in Fig. 1).

Cross-sectional STEM images presented in Fig. 2 with corresponding HRTEM images (inserts) show the size evolution of {113} defects during annealing. It is seen that small clusters (bright dots) are already observed after annealing for 0.5 h and all of them are located within a narrow layer close to the projected range of the O^+ ions (Rp). HRTEM images (inserts in Fig. 2) display, that these are {113} defects including small clusters. Their size increases with annealing time (1 and 1.5 h). The detailed
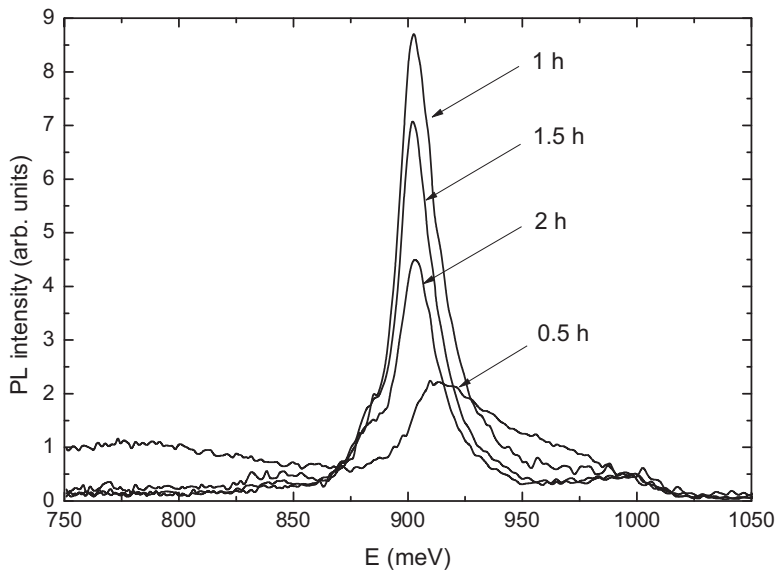
Figure 1 PL spectra under excitation with 532-nm laser light at 78 K of samples implanted with 350 keV oxygen ions at a dose of $3.7 \times 10^{14}\,cm^{-2}$ and then annealed at a temperature of 700 °C in a chlorine-containing atmosphere during various times in the range 0.5–2 h. The excitation power was 56 mW.

HRTEM analysis of the {113} defects in all the samples was carried out using the geometrical phase method (GPA) and is illustrated in Fig. 3. For each sample, a corresponding HRTEM image (upper), map of strain (E_{yy}) distribution (middle) and E_{yy} profile taken across the defect plane (bottom) are displayed in a column. The E_{yy} is a normal component of the elastic deformation tensor along "y" axis. The GPA conditions for calculating the E_{yy} strain map included the following selected **g**-vectors in Fourier space: 002; 00-2; 220; −2-20; 111; −1-1-1; 11-1; −1-11. The mask size − ¼ $\mathbf{g}_{111}$. This algorithm (generalized GPA [19]) makes it possible to increase the signal-to-noise ratio in phase images and the accuracy of strain measurements.

In the case of annealing for 0.5 h (Fig. 3, column a), a small {113} defect with the size of about 3 nm is observed. The positive sign of E_{yy} is assigned to indicate tensile strains (bright contrast) in the defect plane. This strongly suggests that a dominating accumulation of vacancies takes place at initial coarsening stages of {113} defects. The fact that these defects form within a narrow layer close to Rp, where the concentration of implanted ions is maximal, implies interaction of vacancies with oxygen atoms under implantation and their faster release during initial annealing stage relatively clusters catching self-interstitials.

For the 1.0 h annealing (Fig. 3, column b), the enlarged {113} defect displays a sign-alternating E_{yy}, which indicates that the tensile and compressive (dark contrast) strains vary across the defect plane. In this case, we should assume that a mixed accumulation of both vacancies and self-interstitials takes place in the defect plane. Such a possibility of the mixed type {113} defect formation was earlier demonstrated during *in situ* electron irradiation at room temperature in the JEOL4000EX operated at 400 keV [6]. Recently, based on *in situ* and *ex situ* HRTEM data, supported by extensive defect structure modeling and image simulations, we have reviewed all data concerning of the {113} defect nature and concluded that multiple primary clusters (*IV*
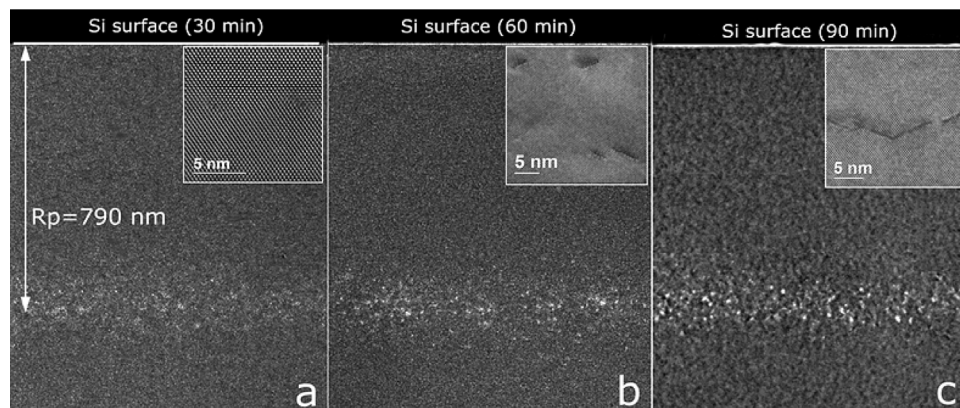

Figure 2 STEM images of a {113} defect distribution in oxygen implanted layer after annealing at a temperature of 700 °C for 0.5 (a), 1 (b), and 1.5 h (c). The inserts display HRTEM images of corresponding {113} defects.
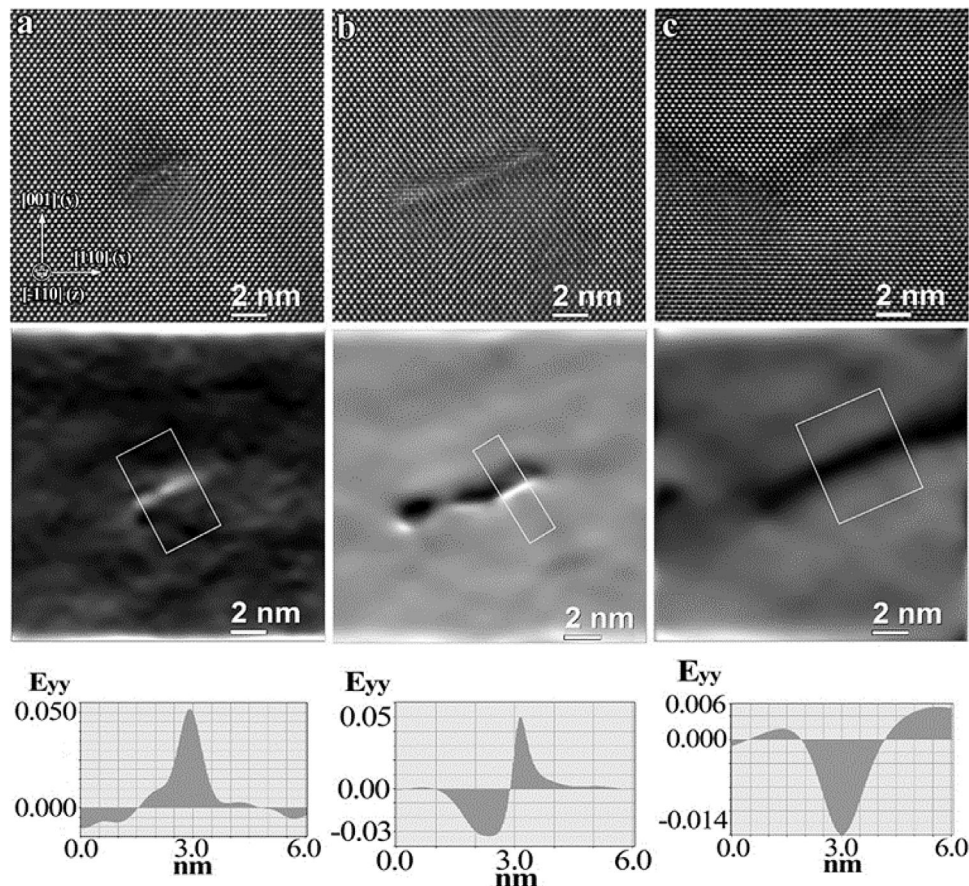
Figure 3 GPA analysis of strains induced by {113} defects in oxygen-implanted layers after annealing at 700 °C for 0.5 h (column a), 1.0 h (column b), and 1.5 h (column c). Each column consists of an HRTEM image (upper), map of strain (E_{yy}) distribution (middle), and E_{yy} profile taken across the defect plane (bottom). The white rectangles show the integration area. HRTEM images were obtained by using Titan 80–300 (a, b) and Jeol 4000RX microscopes (c).

pairs, V_2–$2I$, etc) are ordered in strict sequence along the nearest neighboring atomic chains in the <332> direction constituting the {113} plane to form a universal set topological-bond defects, comprising low-energy (0.7–1 eV/atom) fivefold and eightfold atomic (5–8) rings. The stacked 5–8 array, where all atoms are fully coordinated, provides for defect recombination or incorporation of excessive self-interstitials to build up 5-6$_h$-7-8 topological bond defect structure known as the {113} defect of interstitial type. Such a complex mechanism of point defect aggregation in Si is caused by a low symmetry of primary point defects and results in a decreased crystal energy for any mixed clustering of defects in the {113} plane within a temperature range of $T < 0.5T_{melting}$ [15].

Upon annealing for 1.5 h (Fig. 3, column c), the lattice deformation induced by {113} defects undergoes further transformation. The dark contrast on the map of strains and the negative sign of E_{yy} indicate that compressive strains are dominant in the defect plane, which suggests that the {113} defect of the interstitial type is formed. Note that the HRTEM contrast in the defect plane (Fig. 2c) becomes scattered probably due to the partial defect recombination

and restoration of the crystal structure. This suggests that the transformation observed in the {113} defect structure during the long duration of annealing at 700 °C is responsible for the shift of the PL band peak position from 919 to 903 meV (Fig. 1).

The PL spectra measured in the range of 820–960 meV at different temperatures (5–130 K) for samples implanted with oxygen ions and then annealed for 1 h are shown in Fig. 4. The spectra are dominated by a single R line associated with the {113} defects. The line is asymmetric on the high-energy side. The intensity, peak position, and FWHM of this line noticeably change with the increasing measurement temperature. The second line with energy of nearly 845 meV is observed in the spectra. Its intensity is two orders of magnitude lower than that of R line. The nature of this line is unknown. Separate lines are present in the spectra at energies of 1002, 1033, and 1097 meV, too (not shown in Fig. 4). Their intensities are essentially lower than that of the two lines discussed above.

Figure 5 shows the Arrhenius plots of the luminescence intensity of R line for the sample annealed for 1 h. The dependence of the luminescence intensity on temperature
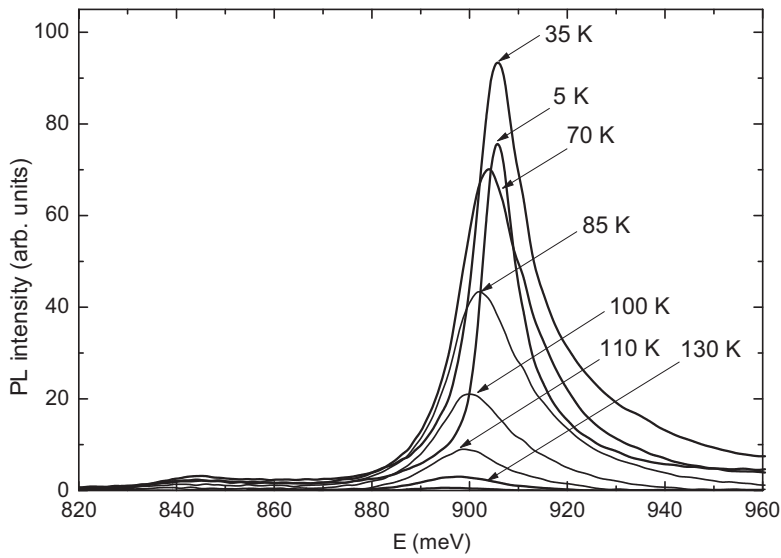
Figure 4 PL spectra measured at different temperatures (5–130 K) for samples implanted with 350 keV oxygen ions at a dose of $3.7 \times 10^{14}\,cm^{-2}$ and then annealed at a temperature of 700 °C in a chlorine-containing atmosphere for 1 h. The excitation power was 56 mW.

(T) is described by the following well-known equation [20]:

$$I = \frac{I_0}{P \cdot f}; \quad P = \left[1 + \frac{C}{1 + A \cdot T^{3/2} \cdot \exp(-W/kT)}\right];$$

$$f = \left[1 + B_1 \cdot T^{3/2} \cdot \exp(-E_1/kT) + B_2 \cdot T^{3/2} \cdot \exp(-E_2/kT)\right],$$

$$(1)$$

where W, E_1, and E_2 are the energies of luminescence enhancement and quenching, C is a quantity involving the ratio of cross sections for exciton capture at luminescence centers and traps, A and B are the interaction constants for this specific center, and k is the Boltzmann constant. At low temperatures, excitons are trapped by shallow-level centers. As the temperature increases, excitons are released and diffuse; then, they are trapped with the subsequent radiative

recombination at the luminescence center. The quenching energies of the luminescence centers are determined by the deactivation of the excited state of the center and by the nonradiative recombination due to the electrically active centers in the forbidden gap. The energies of the enhancement and quenching of the PL intensity of R center and the corresponding parameters are as follows: $W = 19.1$ meV, $E_1 = 32.2$ meV, $E_2 = 175.5$ meV, $A = 74$, $C = 0.2$, $B_1 = 0.11$, and $B_2 = 0.37$. So, the temperature dependence of the intensity of R line was studied here for the first time.

As far as we know, no data related to the temperature enhancement of the luminescence intensity for extended defects have been reported in the literature. The temperature quenching of the luminescence intensity for D1 line of dislocation-related luminescence has been extensively studied [21–26]. In these studies, the temperature quenching of the luminescence intensity was estimated by only a single
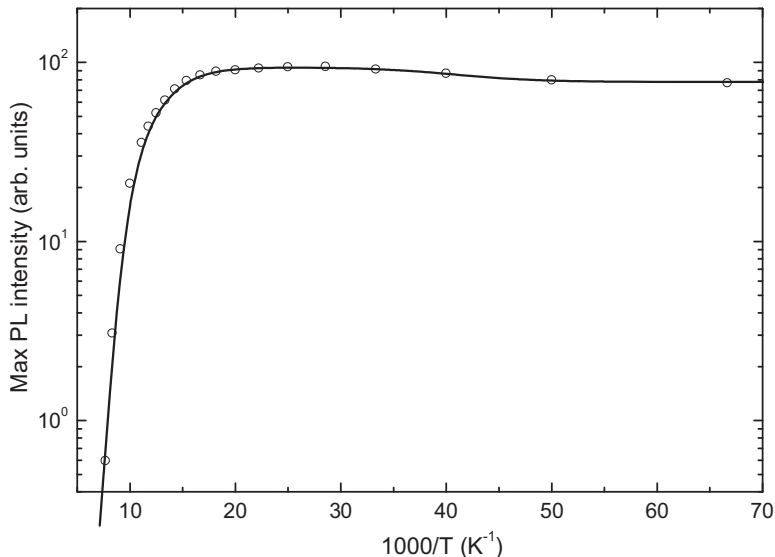

Figure 5 PL intensity of R line for the sample implanted with 350 keV oxygen ions at a dose of $3.7 \times 10^{14}\,cm^{-2}$ and then annealed at a temperature of 700 °C in a chlorine-containing atmosphere for 1 h in relation to the measurement temperature: experimental data, open circles; fitting line, solid curve.
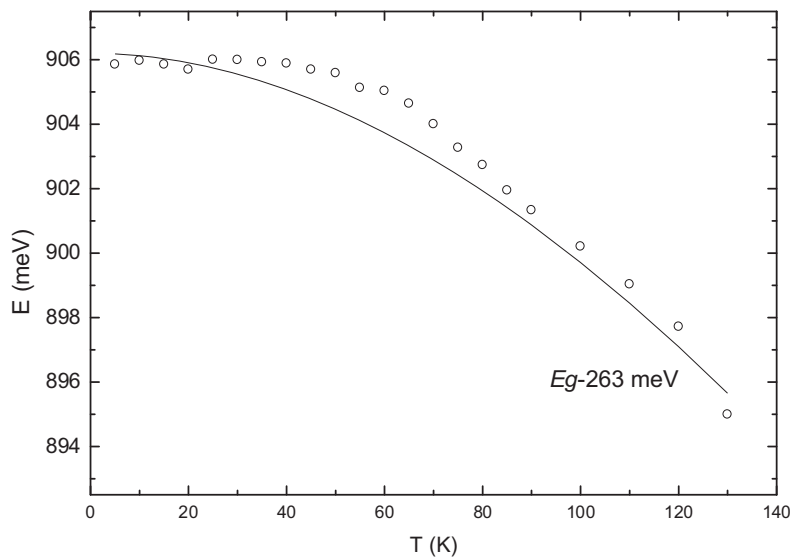
Phys. Status Solidi A 214, No. 7 (2017)

Original
Paper

(6 of 8) 1700317

Figure 6 Measurement temperature dependence of the energy position of R line for the sample implanted with 350 keV oxygen ions at a dose of 3.7×10^{14} cm^{-2} and then annealed at a temperature of 700 °C in a chlorine-containing atmosphere for 1 h: experimental data, open circles; fitting line, solid curve.

quenching energy. In other words, the authors used the modified equation (1):

$$I(T) = \frac{I(0)}{1 + B^* \left(T^{(3/2)}\right) * \exp(-E/(k^*T))}, \quad (2)$$

The authors of [21, 22] found the quenching energy to be 10 and 7 meV, respectively. In contrast, the quenching energies in Refs. [23–26] were in the range 86–180 meV. In heavily dislocated silicon samples studied in Refs. [21, 22], the dislocation-related D1 luminescent line started to rapidly decrease at $T > 30$ K, whereas in Refs. [23–26], its substantial decrease was only observed at $T > 100$ K. Apparently, the samples in the first group contained a high concentration of nonradiative recombination centers in comparison with the samples in the second group. We

emphasize that using equation (1) makes it possible to describe the temperature dependence of the luminescence line intensity more precisely. In particular, we found three energies characterizing the temperature enhancement of the R line intensity (W) and its temperature quenching (E_1 and E_2). Finding two energies E_1 and E_2 indicates that there are two mechanisms of nonradiative recombination in samples containing {113} defects. Another important characteristic of R line is the temperature dependence its energy position (Fig. 6: experimental data, open circles). The solid line was calculated by the equation:

$$E_R(T) = 1.1692 - \frac{4.9 \cdot 10^{-4} \cdot T^2}{T + 655} - 0.263, \quad (3)$$

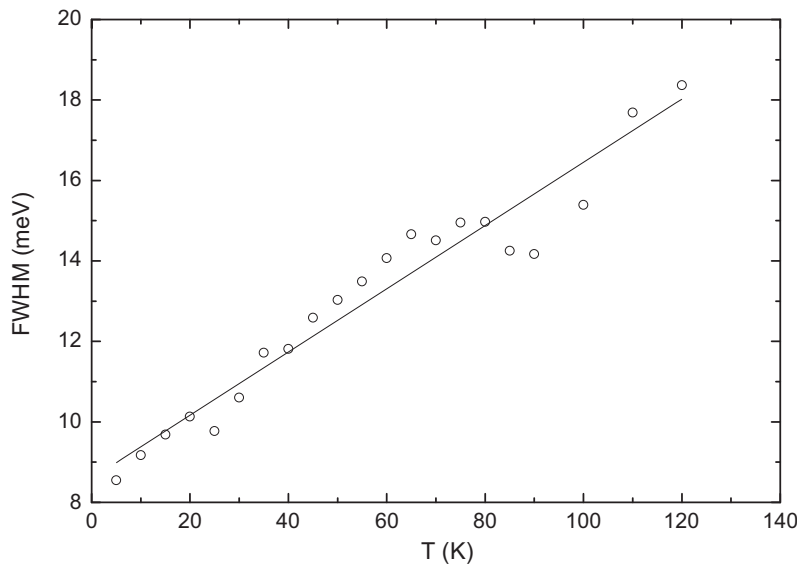where E_R is the energy position of R line (eV) and T is the

Figure 7 Measurement temperature dependence of the FWHM of R line for the sample implanted with 350 keV oxygen ions at a dose of 3.7×10^{14} cm^{-2} and then annealed at a temperature of 700 °C in a chlorine-containing atmosphere for 1 h: experimental values, open circles; fitting line, solid curve.

measurement temperature (K). This equation presents the temperature dependence of the energy gap in Si (Eg) [27], reduced by 0.263 eV. In the other words, $E_R(T) = Eg - 0.263$. It can be seen that the experimental data are well described by equation (3). For the oxygen-implanted sample annealed for 1 h, the peak position of R line remains unchanged in the temperature range 5–40 K and starts to be redshifted at higher temperatures. The observed behavior of the position of R line has not been reported before. The trend exhibited by the R peak energy in the temperature dependence corresponds to the motion of the band gap with temperature. The similar temperature dependence of the peak energy was early observed for the D1 and D2 dislocation-related lines [26, 28, 29]: their energy positions move in parallel with the band gap.

The dependence of the FWHM of R line in the oxygen-implanted sample annealed for 1 h is shown in Fig. 7, with the experimental data represented by open circles. The FWHM is 14 meV at 78 K and is well correlated with published data [9–12, 16]. The FWHM of R line (in meV) grows with increasing temperature and is rather well described by the equation:

$$FWHM(T) = 8.6 + 0.079 \cdot T. \tag{4}$$

The temperature increase in the FWHM of R line can be accounted for by the fact that it is constituted by two narrower lines in a certain temperature range, as observed in Refs. [5, 10]. A temperature-induced increase in the FWHMs of the D1 and D2 dislocation-related lines associated with other extended defects formed from self-interstitials in silicon has been observed previously [28].

4 Summary A direct correlation between the transformation of PL spectra and lattice deformations induced by {113} defects in n-Cz-Si (100) wafers by implantation with oxygen ions, and subsequent annealing at various annealing durations has been revealed. The type of {113} defects was examined by the generalized geometrical-phase method integrated with Digital Micrograph (GATAN) program [19] for analysis of the lattice deformations on the basis of the HRTEM images of these defects. This analysis revealed the appearance of the tensile strains in the {113} defect planes in samples upon their annealing for 0.5 h, sign-alternating stress profile after 1 h, and compressive strains after 1.5 h. This means that raising the annealing time from 0.5 to 1.5 h is followed by the formation of vacancy-type, mixed (interstitial-vacancy) and interstitial {113} defects. The transformation of the vacancy (113) defects into interstitial-vacancy defects leads to a redshift of the PL band. The formation of interstitial defects is followed by a decrease in the R line intensity. The behavior of the main parameters of R line with the measurement temperature was studied for the first time and their analytical temperature dependences were found. It is important to point out a similar behavior of luminescence parameters of {113} defects and dislocation-related centers

in dependence on temperature. Both extended defects exhibit microwave conductivity and electric-dipole spin-resonance [31, 32]. However, the positions and the origin of electrically active energy levels responsible for rod-like and dislocation-related luminescence is at present unclear [10, 20–22, 30–33]. Much effort is to be undertaken in studying the ion-implanted silicon in order to understand which real atomic structures of the {113} defect correspond to various annealing stages.

References

[1] G. Z. Pan, R. P. Ostroumov, L. P. Ren, Y. G. Lian, and K. L. Wang, J. Non-Cryst. Solids **352**, 2506 (2006).

[2] H. Bender and J. Vanhellemont, Phys. Status Solidi A **107**, 455 (1988).

[3] S. Takeda, Jap. J. Appl. Phys. **30**, L639 (1991).

[4] M. Tajima, U. Gosele, J. Weber, and R. Sauer, Appl. Phys. Lett. **43**, 270 (1983).

[5] L. Jeyanathan, E. C. Lightowlers, V. Higgs, and G. Davies, Mater. Sci. Forum **143-147**, 1499 (1994).

[6] L. Fedina, A. Gutakovskii, A. Aseev, J. Van Landuyt, and J. Vanhellemont, Phys. Status Solidi A **171**, 147 (1999).

[7] N. E. B. Cowern, K. T. F. Janssen, and H. F. F. Jos, J. Appl. Phys. **68**, 6191 (1990).

[8] D. J. Eaglesham, P. A. Stolk, H.-J. Gossmann, and J. M. Poate, Appl. Phys. Lett. **65**, 2305 (1994).

[9] S. Coffa, S. Libertino, and C. Spinella, Appl. Phys. Lett. **76**, 321 (2000).

[10] D. C. Schmidt, B. G. Svensson, M. Seibt, C. Jagadish, and G. Davies, J. Appl. Phys. **88**, 2309 (2000).

[11] P. K. Giri, Semicond. Sci. Technol. **20**, 638 (2005).

[12] Y. Yang, J. Bao, C. Wang, and M. J. Aziz, J. Appl. Phys. **107**, 123109 (2010).

[13] S. Charnvanichborikarn, J. Wong-Leung, C. Jagadish, and J. S. Williams, MRS Commun. **2**, 101, (2012).

[14] P. A. Stolk, H. J. Gossmann, D. J. Eaglesham, D. C. Jacobson, C. S. Rafferty, G. H. Gilmer, M. Jaraiz, J. M. Poate, H. S. Luftman, and T. E. Haynes, J. Appl. Phys. **81**, 6031 (1997).

[15] L. I. Fedina, A. K. Gutakovskii, A. V. Latyshev, and A. L. Aseev, in: Advances in Semiconductor Nanostructures, Growth, Characterization, Properties and Applications, edited by A. Latyshev, A. Dvurechenskii, and A. Aseev, (Elsevier, Amsterdam, 2016), pp. 383–408.

[16] N. A. Sobolev, A. E. Kalyadin, P. N. Aruev, V. V. Zabrodskii, E. I. Shek, K. F. Shtel'makh, and K. V. Karabeshkin, Phys. Solid State **58**, 2499 (2016).

[17] J. F. Ziegler, M. D. Ziegler, and J. P. Biersack, Nucl. Instrum. Methods B **268**, 1818 (2010).

[18] M. J. Hytch, E. Snoeck, and R. Kilaas, Ultramicroscopy **74**, 131 (1998).

[19] A. K. Gutakovskii, A. L. Chuvilin, and S. A. Song, Bull. Russian Acad. Sci.: Phys. **71**, 1426 (2007).

[20] G. Davies, Phys. Rep. **176**, 83 (1989).

[21] M. Suezawa, Y. Sasaki, and K. Sumino, Phys. Status Solidi A **79**, 173 (1983).

[22] R. Sauer, J. Weber, J. Stolz, E. R. Weber, K. H. Kurster, and H. Alexander, Appl. Phys. A **36**, 1 (1985).

[23] V. V. Kveder, E. A. Steinman, S. A. Shevchenko, and H. G. Grimmeiss, Phys. Rev. B **51**, 10520 (1995).

[24] E.Ö. Sveinbjörnsson and J. Weber, Mater. Res. Soc. Symp. Proc. **422**, 148 (1996).

[25] N. A. Sobolev, O. B. Gusev, E. I. Shek, V. I. Vdovin, T. G. Yugova, and A. M. Emel'yanov, J. Luminesc. **80**, 357 (1999).

[26] L. Xang, D. Li, L. Jin, S. Wang, and D. Yang, J. Appl. Phys. **113**, 033518 (2013).

[27] V. Alex, S. Finkbeiner, and J. Weber, J. Appl. Phys. **79**, 6943 (1996).

[28] S. Binetti, S. Pizzini, E. Leoni, R. Somaschini, A. Castaldini, and A. Cavallini, J. Appl. Phys. **92**, 2437 (2002).

[29] V. Kveder, M. Badylevich, E. Steinman, A. Izotov, M. Seibt, and W. Schroter, Appl. Phys. Lett. **84**, 2106 (2004).

[30] N. A. Sobolev, Semiconductors **44**, 3 (2010).

[31] T. Mchedlidze, S. Binetti, A. Le Donne, S. Pizzini, and M. Suezawa, J. Appl. Phys. **98**, 043507 (2005).

[32] T. Mtchedlidze, T. Arguirov, G. Jia, and M. Kittler, Phys. Status Solidi A, **204**, 2229 (2007).

[33] R. Jones, Solid State Phenom. **131-133**, 225 (2008).